Supporting Information for

Binary pentagonal auxetic materials for photocatalysis and energy storage with outstanding performances

Zishuang Cheng,[a,b] Xiaoming Zhang,[a,b,c]* Hui Zhang,[a,b] Heyan Liu,[a,b,c] Xiao Yu,[a,b] Xuefang Dai,[a,b] Guodong Liu,[a,b]* and Guifeng Chen[a,b]*

[a]State Key Laboratory of Reliability and Intelligence of Electrical Equipment, Hebei University of Technology, Tianjin 300130, China.

[b]School of Materials Science and Engineering, Hebei University of Technology, Tianjin 300130, China.

[c]State Key Laboratory of Baiyunobo Rare Earth Resource Researches and Comprehen sive Utilization, Baotou Research Institute of Rare Earths, Baotou 014030, China.

*Corresponding authors:

Xiaoming Zhang, zhangxiaoming87@hebut.edu.cn;

Guodong Liu, gdliu1978@126.com;

Guifeng Chen, cgfchen@hebut.edu.cn.

Contents of Supporting Information

The absorption coefficient:

The optical properties usually rely on the complex dielectric function (frequency) for characterization, which is defined as:

$$\varepsilon(\omega) = \varepsilon_1(\omega) + i\varepsilon_2(\omega) \quad (1)$$

therein $\varepsilon_1(\omega)$ and $\varepsilon_2(\omega)$ represent the real and imaginary parts, respectively. The imaginary part [$\varepsilon_2(\omega)$] of the dielectric function can be expressed as [1]:

$$\varepsilon_2(\omega) = \frac{4\pi e^2}{m^2\omega^2}\sum_{i,f}\int \frac{2d^3k}{(2\pi)^3}|\langle ik|P|fk\rangle|^2 F_i^k\left(1 - F_f^k\right)\delta\left(E_f^k - E_i^k - E\right) \quad (2)$$

where ω, E and F are incident photon frequency, incident photon energy and the Fermi function, respectively. P, $|ik\rangle$ and $|fk\rangle$ represent the transition matrix, the CB state and VB state, respectively. Besides, based on the Kramers-Kronig transformation [2], the real part [$\varepsilon_1(\omega)$] can be described by the following equation:

$$\varepsilon_1(\omega) = 1 + (\frac{2}{\pi})p\int_0^\infty d\omega' \frac{(\omega')^2\varepsilon_2(\omega)}{(\omega')^2 - (\omega)^2} \quad (3)$$

here p is the integral principal value. More importantly, the absorption coefficient [$\alpha(\omega)$] can be calculated by [3]:

$$\alpha(\omega) = \frac{\sqrt{2\omega}}{c}[\sqrt{\varepsilon_1^2(\omega) + \varepsilon_2^2(\omega)} - \varepsilon_1(\omega)]^{1/2} \quad (4)$$

where c is the speed of light in vacuum.

The carrier mobility:

The carrier effective mass (m^*) can be obtained by fitting the electronic band dispersion as the following equation [4]:

$$\frac{1}{m^*} = \frac{1}{\hbar^2}\frac{\partial^2 E(k)}{\partial k^2} \quad (5)$$

where $\hbar$ is the reduced Plank constant, k represents the wave vector and $E(k)$ represents the carrier energy. Based on the deformation potential theory, the carrier mobility can be assessed by the following formula [5]:

$$\mu = \frac{e\hbar^3 C_{2D}}{k_B T m_e^* m_d E_d^2} \quad (6)$$

where k_B is the Boltzmann constant and T is the temperature (300 K). m_e^* is the effective mass of electrons or holes along the transport direction. m_d is the average effective mass defined using the expression $m_d = \sqrt{m_x^* m_y^*}$ where m_x^* and m_y^* are along the *x* and *y* directions, respectively. E_d represents the deformation potential constant, which is defined as $E_d = \frac{\partial E_{edge}}{\partial \delta}$ where E_{edge} represents the shift of the band edge position with respect to the uniaxial strain δ. C_{2D} is the elastic modulus, which can be determined by $C_{2D} = \frac{1}{S_0} \frac{\partial^2 E}{\partial \delta^2}$, where E is the total energy of monolayer after deformation and S_0 is the lattice area of monolayer under equilibrium.

[1] M. Naseri and J. Jalilian. Electronic and optical investigations of Be_2C monolayer: Under stress and strain conditions, *Mater. Res. Bull.* 88 (2017) 49-55.

[2] A.B. Kuzmenko. Kramers–Kronig constrained variational analysis of optical spectra, *Rev. Sci. Instrum.* 76 (2005) 083108.

[3] S. Saha, T.P. Sinha and A. Mookerjee. Electronic structure, chemical bonding, and optical properties of paraelectric $BaTiO_3$, *Phys. Rev. B* 62 (2000) 8828.

[4] Q. Zhang, X. Wang and S.L. Yang. δ-SnS: An Emerging Bidirectional Auxetic Direct Semiconductor with Desirable Carrier Mobility and High-Performance Catalytic Behavior toward the Water-Splitting Reaction, *ACS Appl. Mater. Interfaces* 13 (2021) 31934-31946.

[5] J. Bardeen and W. Shockley. Deformation potentials and mobilities in non-polar crystals, *Phys. Rev.* 80 (1950) 72.

Table S1 Calculated lattice parameters for Penta-C_nX_{6-n}: a is lattice constant, d is the thickness in vertical direction, d_{C-X} is the bond length of C-X, ΔH is the formation enthalpy of Penta-C_nX_{6-n}.

Materials (Penta-)	a (Å)	d (Å)	d_{C-X} (Å)	ΔH (eV/atom)
C_5B	3.771	1.109	1.606	1.014
C_4B_2	4.004	0.807	1.643	1.074
C_2B_4	3.934	1.073	1.582	0.610
CB_5	4.106	0.894	1.559	0.884
C_5N	3.534	1.356	1.541	1.194
C_4N_2	3.415	1.509	1.514	1.485
C_2N_4	3.313	1.529	1.468	0.610
CN_5	3.250	1.814	1.430	1.375
C_5Al	4.063	1.353	1.921	1.298
C_4Al_2	4.668	1.444	2.061	0.743
C_2Al_4	5.110	1.189	1.975	0.595
CAl_5	5.648	1.491	1.961	0.792
C_5Si	4.022	1.272	1.817	0.988
C_4Si_2	4.409	1.326	1.908	0.605
C_2Si_4	4.217	2.253	1.883	0.741
CSi_5	4.727	2.401	1.904	0.719
C_5P	3.891	1.331	1.758	0.925
C_4P_2	4.141	1.409	1.794	0.672
C_2P_4	4.092	2.319	1.879	0.174
CP_5	4.479	2.622	1.948	0.229
C_5Ga	4.096	1.349	1.929	1.458
C_4Ga_2	4.721	1.434	2.086	0.952
C_2Ga_4	5.010	1.568	2.010	0.797
CGa_5	5.570	1.634	2.005	0.654
C_5Ge	4.105	1.294	1.877	1.257
C_4Ge_2	4.575	1.365	1.993	0.915
C_2Ge_4	4.575	2.337	2.012	0.854
CGe_5	5.098	2.518	2.003	0.728
C_5As	4.024	1.386	1.869	1.339
C_4As_2	4.423	1.520	1.944	1.280
C_2As_4	4.362	2.541	2.015	0.522
CAs_5	4.730	2.891	2.043	0.535

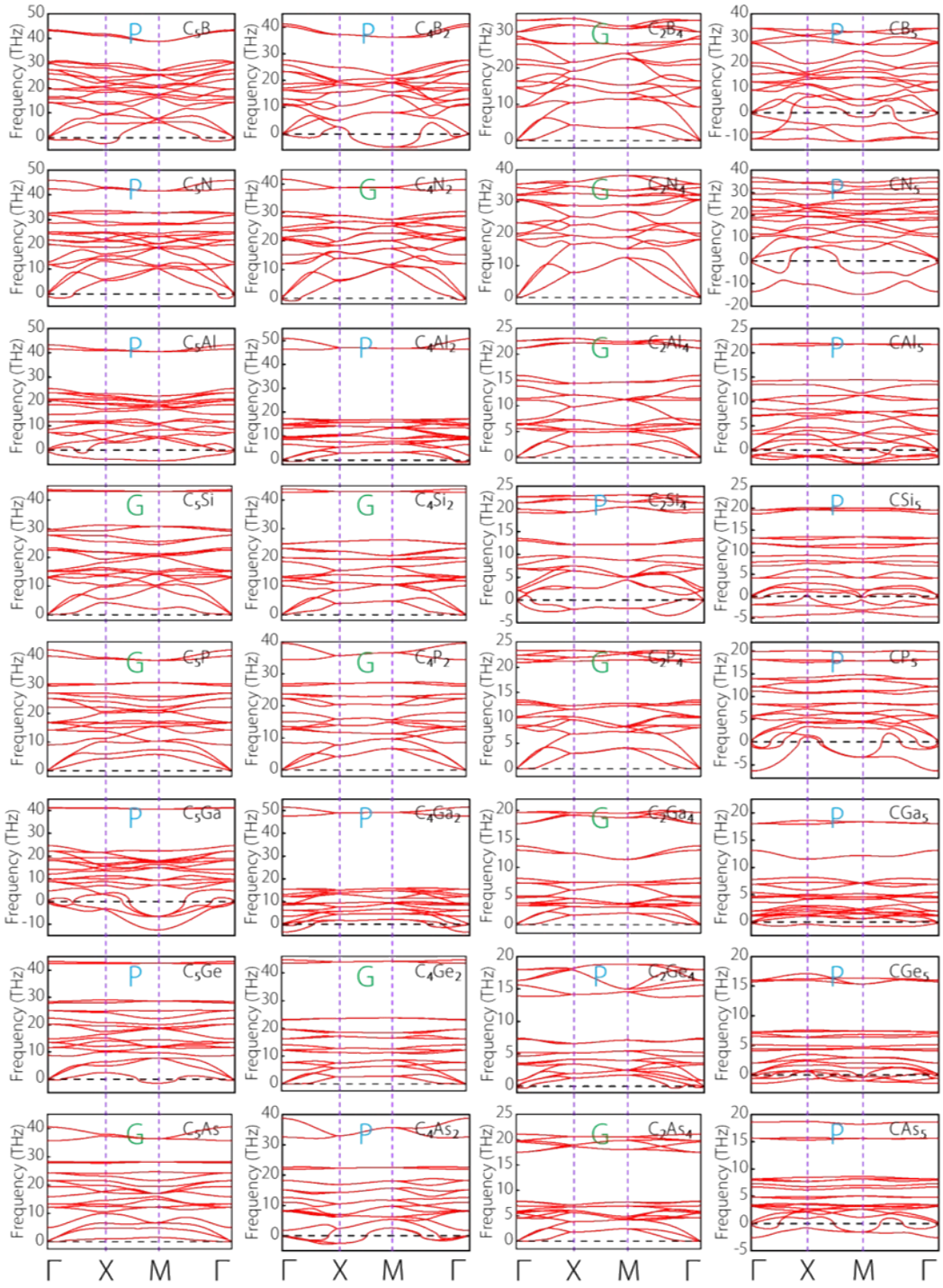

Figure S1 Phonon spectra of Penta-C_nX_{6-n}. G (green) and P (blue) represent the good and poor dynamic stability, respectively. The dashed line indicates zero frequency, below which the structure is dynamically unstable.

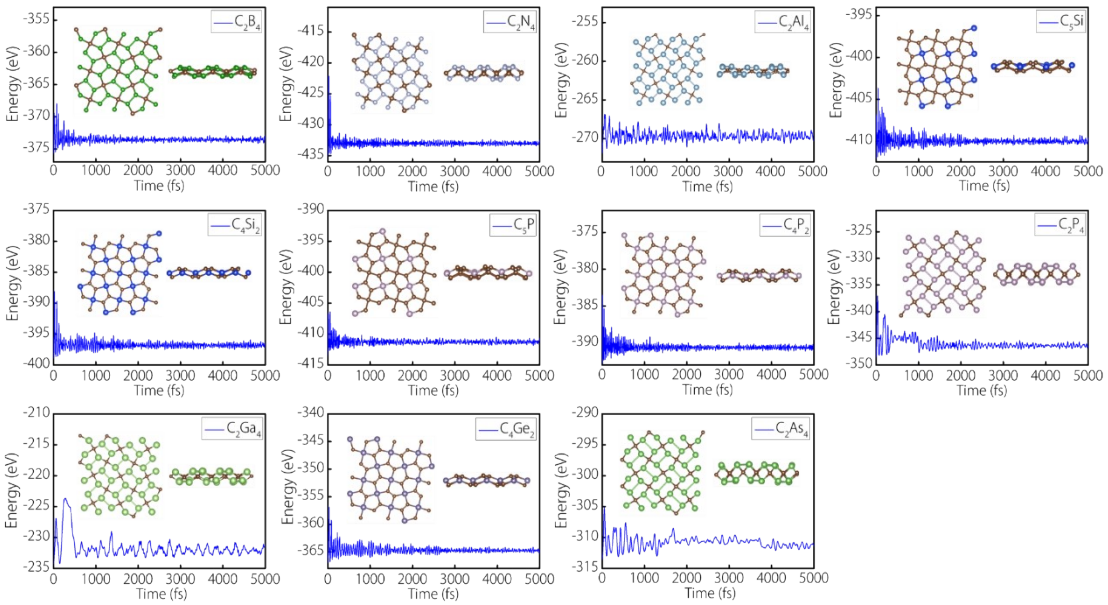

Figure S2 Evolutions of total potential energy of Penta-C_nX_{6-n} with respect to simulation time at the temperature of 300 K, and the top and side views of snapshots after 5000 fs.

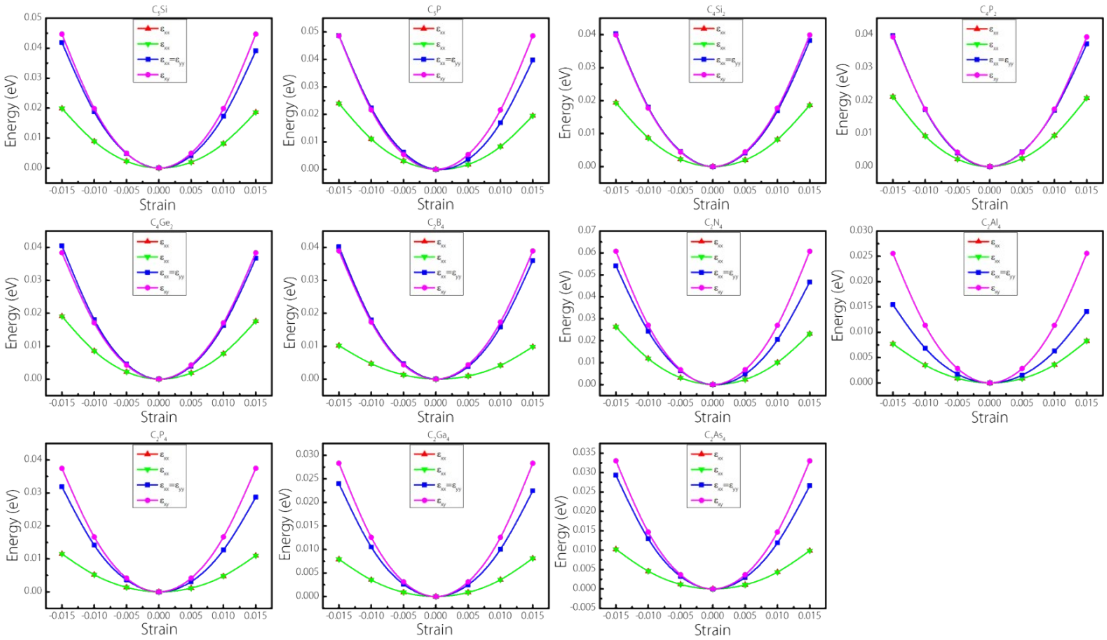

Figure S3 Elastic energies of Penta-C_nX_{6-n} under uniaxial, biaxial and shear in-plane strains, respectively.

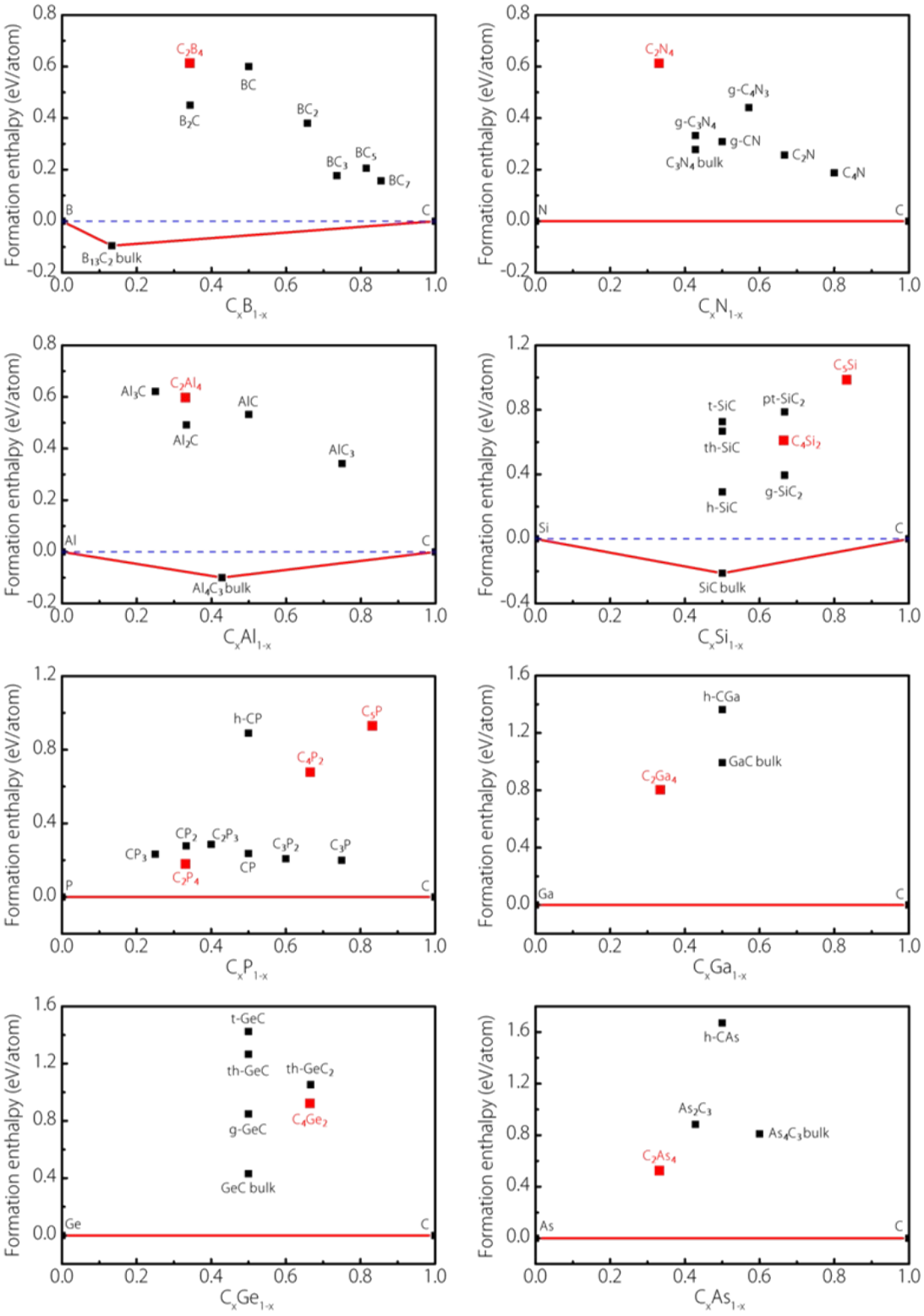

Figure S4 Formation enthalpies of stable Penta-C_nX_{6-n} compared with their allotropes in other works. Therein, the red marks are our Penta-C_nX_{6-n} and the black ones are others. References are as follows: $B_{13}C_2$ bulk, C_3N_4 bulk, Al_4C_3 bulk, GaC bulk, As_4C_3 bulk [6]; B_2C, BC, BC_2, BC_3, BC_5, BC_7 [7-11]; g-C_3N_4, g-CN, g-C_4N_3, C_2N, C_4N [12-16]; Al_3C, Al_2C, AlC, AlC_3 [17]; h-SiC, th-SiC, t-SiC, g-SiC_2, pt-SiC_2 [18-20]; CP_3,

CP_2, C_2P_3, CP, h-CP, C_3P_2, C_3P [21-23]; h-CGa [23]; g-GeC, th-GeC, t-GeC, th-GeC_2 [18,24,25]; h-CAs, As_2C_3 [23,26].

[6] A. Jain, S.P. Ong, G. Hautier, W. Chen, W.D. Richards, S. Dacek, et al., Commentary: The Materials Project: A materials genome approach to accelerating materials innovation, *APL Mater.* 1 (2013) 011002.
APL Materials, 2013, 1(1), 011002.

[7] X.J. Wu, Y. Pei, X.C. Zeng, B_2C graphene, nanotubes, and nanoribbons, *Nano Lett.* 9 (2009) 1577-1582.

[8] D. Das, R.P. Hardikar, S.S. Han, K.R. Lee, A.K. Singh, Monolayer BC_2: an ultrahigh capacity anode material for Li ion batteries, *Phys. Chem. Chem. Phys.* 19 (2017) 24230-24239.

[9] C. Oshima, BC_x layers with honeycomb lattices on an NbB_2 (0001) surface, *J. Phys. Condens. Matter* 24 (2012) 314206.

[10] B.M. Way, J.R. Dahn, T. Tiedje, K. Myrtle, M. Kasrai, Preparation and characterization of B_xC_{1-x} thin films with the graphite structure, *Phys. Rev. B* 46 (1992) 1697.

[11] K. Belasfar, A.E. Kenz, A. Benyoussef, First-principles study of BC_7 monolayer an ultra-high capacity anode for lithium-ion and sodium-ion batteries applications, *Mater. Chem. Phys.* 257 (2021) 123751.

[12] X.C. Wang, K. Maeda, A. Thomas, K. Takanabe, G. Xin, K. Domen, M. Antonietti, A metal-free polymeric photocatalyst for hydrogen production from water under visible light, Nat. Mater. 8 (2009) 76-82.

[13] J. Li, C.B. Cao, J.W. Hao, H.L. Qiu, Y.J. Xu, H.S. Zhu, Self-Assembled One-Dimensional Carbon Nitride Architectures, *Diamond Relat. Mater.* 2006, 15, 1593-1600.

[14] J.S. Lee, X.Q. Wang, H.M. Luo, S. Dai, Fluidic carbon precursors for formation of functional carbon under ambient pressure based on ionic liquids, *Adv. Mater.* 22 (2010) 1004-1007.

[15] S. Guan, Y.C. Cheng, C. Liu, J.F. Han, Y.H. Lu, S.A. Yang, et al., Effects of strain

on electronic and optic properties of holey two-dimensional C_2N crystals, *Appl. Phys. Lett.* 107 (2015) 231904.
[16] C.Y. Pu, D.W. Zhou, Y.F. Li, H.Y. Liu, Z.F. Chen, Y.C. Wang, et al., Two-dimensional C_4N global minima: unique structural topologies and nanoelectronic properties, *J. Phys. Chem. C* 121 (2017) 2669-2674.
[17] J. Dai, X.J. Wu, J.L. Yang, X.C. Zeng, Al_xC monolayer sheets: two-dimensional networks with planar tetracoordinate carbon and potential applications as donor materials in solar cell, *J. Phys. Chem. Lett.* 5 (2014) 2058-2065.
[18] M.E. Kilic, K.R. Lee, Tetrahex carbides: Two-dimensional group-IV materials for nanoelectronics and photocatalytic water splitting, *Carbon*, 174 (2021) 368-381.
[19] L.J. Zhou, Y.F. Zhang, L.M. Wu, SiC_2 siligraphene and nanotubes: novel donor materials in excitonic solar cells, *Nano Lett.* 13 (2013) 5431-5436.
[20] Y.F. Li, F.Y. Li, Z. Zhou, Z.F. Chen, SiC_2 silagraphene and its one-dimensional derivatives: where planar tetracoordinate silicon happens, *J. Am. Chem. Soc.* 133 (2011) 900-908.
[21] M. Kar, R. Sarkar, S. Pal, P. Sarkar, Two-dimensional CP_3 monolayer and its fluorinated derivative with promising electronic and optical properties: A theoretical study, *Phys. Rev. B* 10 (2020) 195305.
[22] G.X. Wang, R. Pandey, S.P. Karna, Carbon phosphide monolayers with superior carrier mobility, *Nanoscale*, 8 (2016) 8819-8825.
[23] S, Kansara, S.K. Gupta, Y. Sonvane, Boltzmann transport properties of ultra thin-layer of h-CX monolayers. *AIP Conf. Proc.* 1951 (2018) 020007.
[24] N. Khossossi, A. Banerjee, I. Essaoudi, A. Ainane, P. Jena, R. Ahuja, Thermodynamics and kinetics of 2D g-GeC monolayer as an anode material for Li/Na-ion batteries. *J. Power Sources*, 485 (2021) 229318.
[25] W. Zhang, C.C. Chai, Q.Y. Fan, M.L. Sun, Y.X. Song, Y.T. Yang, et al., Two-Dimensional Tetrahex-GeC_2: A Material with Tunable Electronic and Optical Properties Combined with Ultrahigh Carrier Mobility, *ACS Appl. Mater. Interfaces* 13 (2021) 14489-14496.
[26] P.F. Liu, T. Bo, Z.F. Liu, O. Eriksson, F.W. Wang, J.J. Zhao, et al., Hexagonal M_2C_3 (M= As, Sb, and Bi) monolayers: New functional materials with desirable band gaps and ultrahigh carrier mobility, *J. Mater. Chem. C* 6 (2018) 12689-12697.

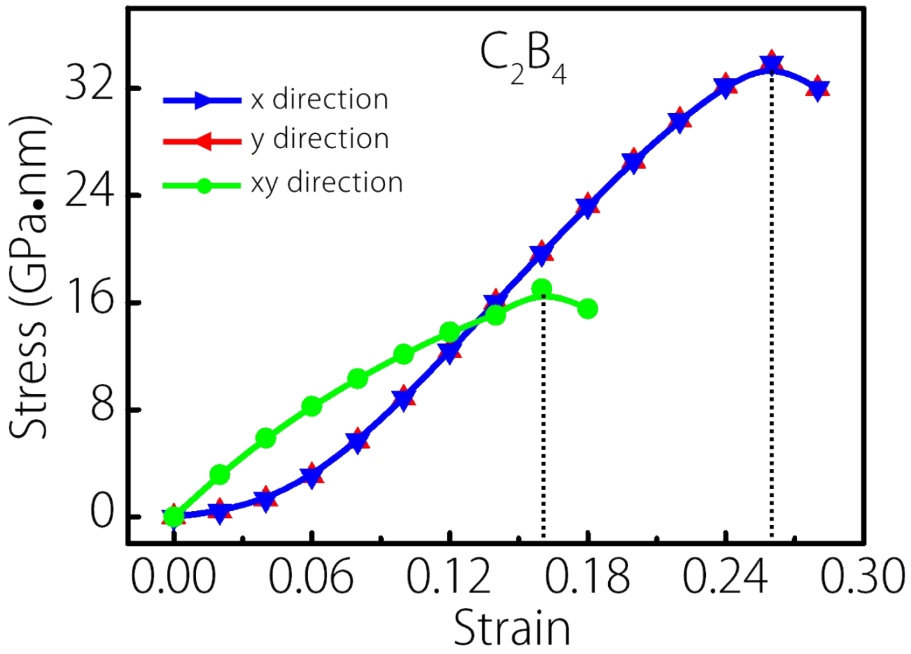

Figure S5 Stress-strain relationships of uniaxial (*x* and *y* directions) and biaxial (*xy* direction) in-plane strains for Penta-C_2B_4.

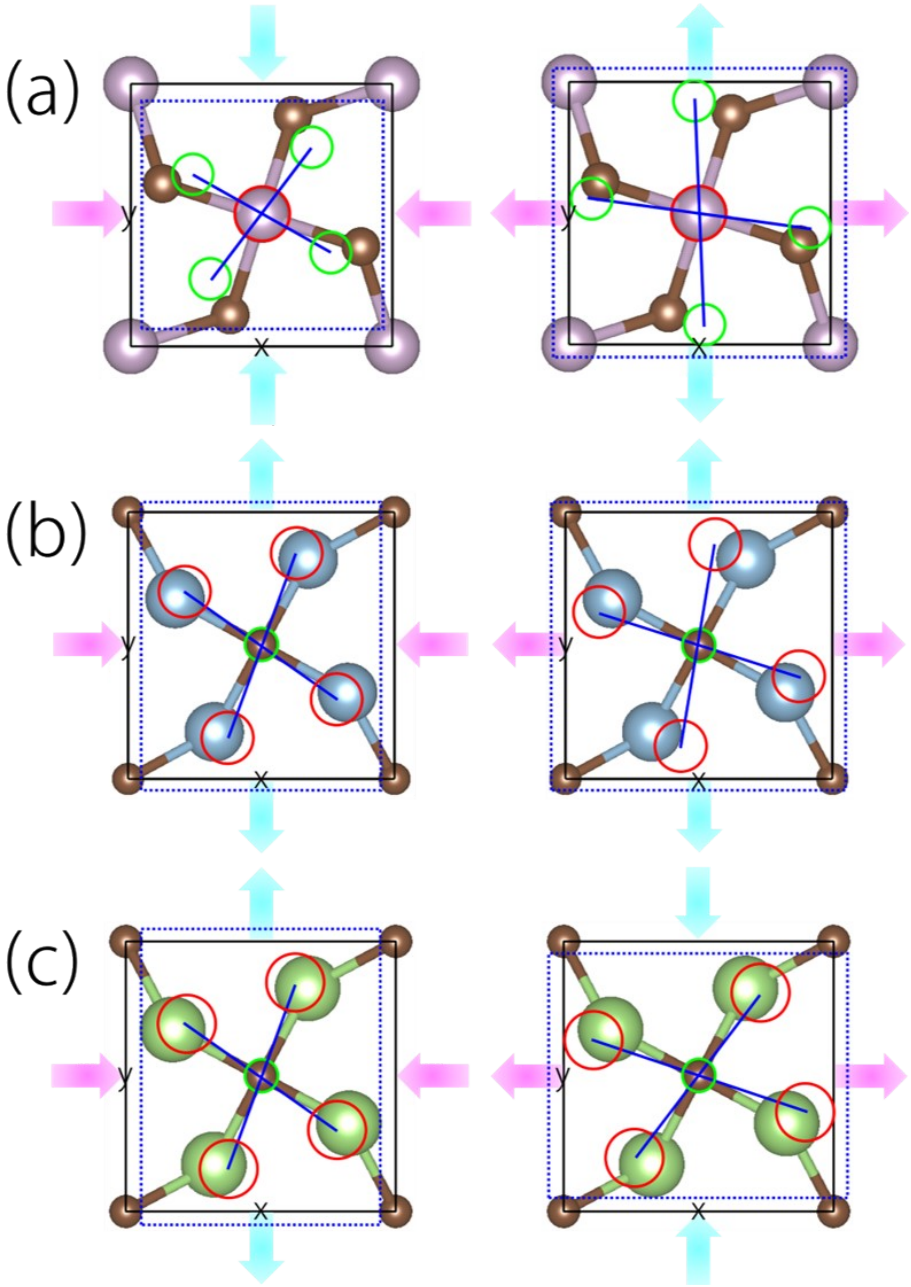

Figure S6 Evolutions of the local skeleton configurations of (a) Penta-C_4P_2 (NPR), (b) Penta-C_2Al_4 (H-NPR) and (c) Penta-C_2Ga_4 (PRR) under the uniaxial strain along *x* direction. The pink and cyan arrows indicate the applied and driven uniaxial strains.

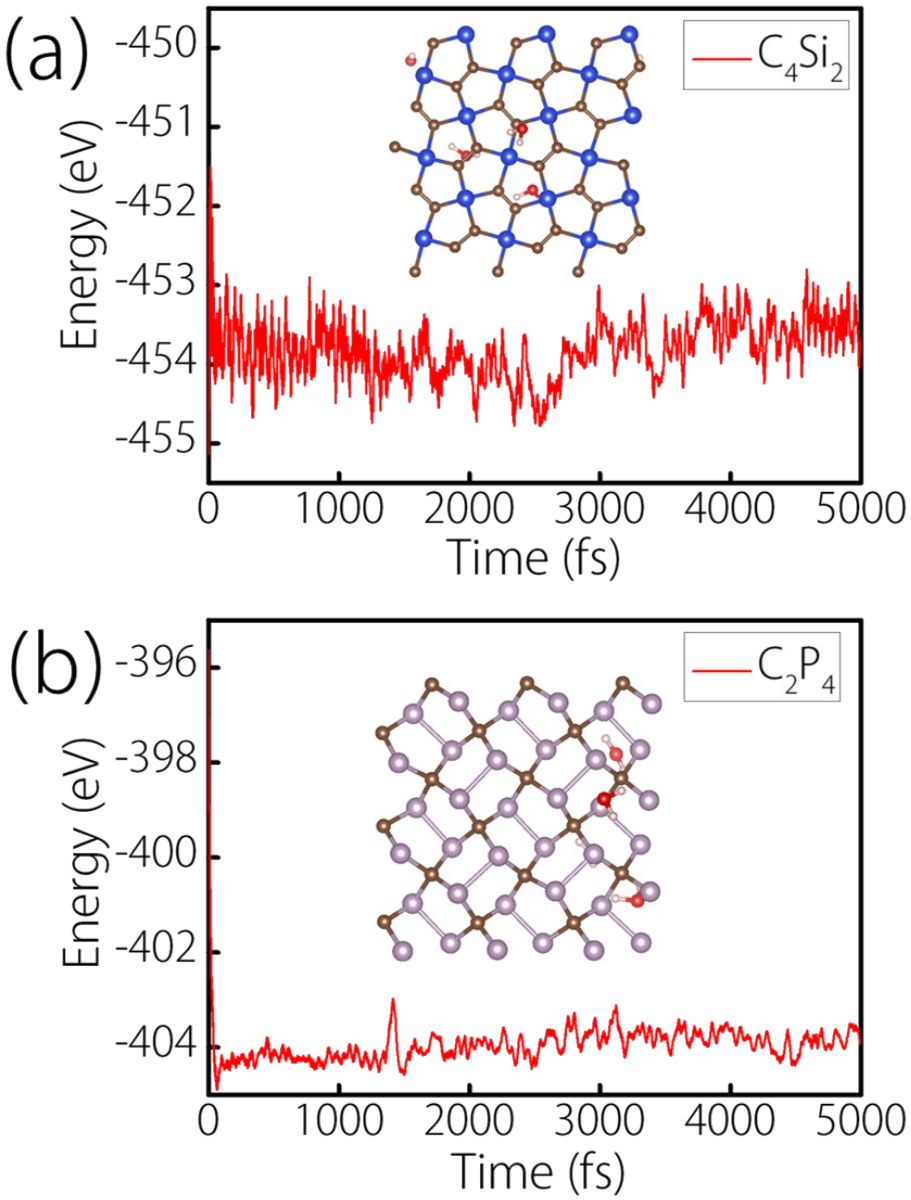

Figure S7 Evolution of the total energy of Penta-C_4Si_2 and Penta-C_2P_4 (3×3 supercells) obtained from 5000 fs AIMD simulations in a 300 K water environment. And the final configuration at t = 5000 fs is shown in the inset for comparison.

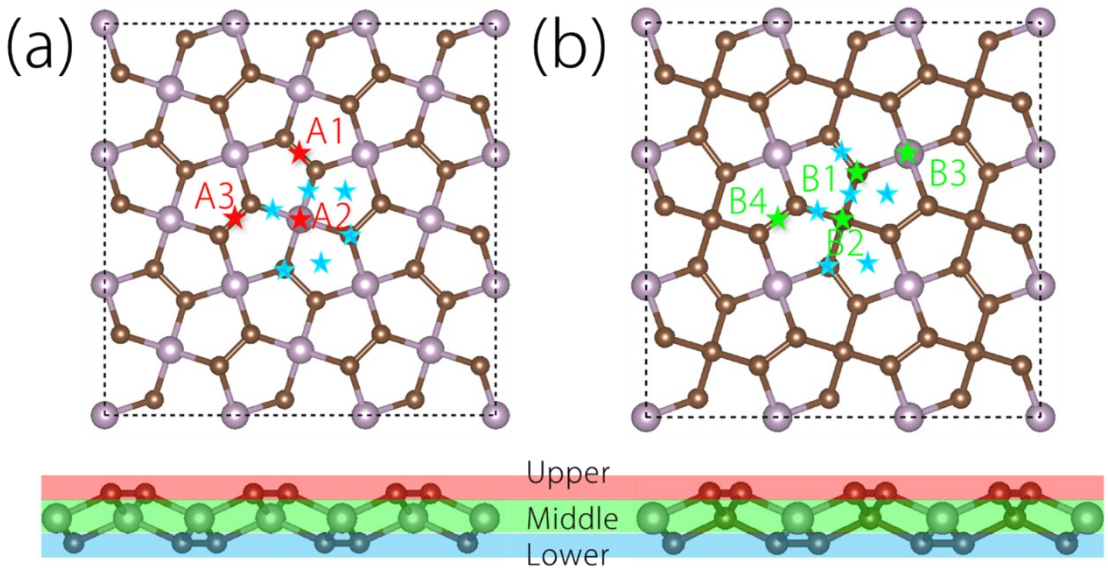

Figure S8 Possible adsorption sites on (a) Penta-C_4P_2 and (b) Penta-C_5P. Therein, A1 (on the bridge site of the lower C atoms), A2 (on the top site of the P atoms) and A3 (on the bridge site of the upper C atoms) are stable adsorption sites for Penta-C_4P_2; B1 (on the top site of the lower C atoms), B2 (on the top site of the middle C atoms), B3 (on the top site of the P atoms) and B4 (on the bridge site of the upper C atoms) are stable adsorption sites for Penta-C_5P. The blue stars represent the unstable adsorption sites (the Na atoms at these sites would move to the stable sites after structural optimization).